ORIGINAL ARTICLE

Quantitative Magnetic Resonance Imaging of Bronchopulmonary Dysplasia in the Neonatal Intensive Care Unit Environment

Laura L. Walkup[1], Jean A. Tkach[2], Nara S. Higano[1,3], Robert P. Thomen[1,3], Sean B. Fain[4], Stephanie L. Merhar[5], Robert J. Fleck[6], Raouf S. Amin[7], and Jason C. Woods[1,3]

[1]Center for Pulmonary Imaging Research, Division of Pulmonary Medicine, Department of Radiology, [2]Imaging Research Center, Department of Radiology, [5]Division of Neonatology and Pulmonary Biology, [6]Department of Radiology, and [7]Division of Pulmonary Medicine, Cincinnati Children's Hospital Medical Center, Cincinnati, Ohio; [3]Department of Physics, Washington University in St. Louis, St. Louis, Missouri; and [4]Department of Medical Physics, University of Wisconsin, Madison, Wisconsin

Abstract

Rationale: Bronchopulmonary dysplasia (BPD) is a prevalent yet poorly characterized pulmonary complication of premature birth; the current definition is based solely on oxygen dependence at 36 weeks postmenstrual age without objective measurements of structural abnormalities across disease severity.

Objectives: We hypothesize that magnetic resonance imaging (MRI) can spatially resolve and quantify the structural abnormalities of the neonatal lung parenchyma associated with premature birth.

Methods: Using a unique, small-footprint, 1.5-T MRI scanner within our neonatal intensive care unit (NICU), diagnostic-quality MRIs using commercially available sequences (gradient echo and spin echo) were acquired during quiet breathing in six patients with BPD, six premature patients without diagnosed BPD, and six full-term NICU patients (gestational ages, 23–39 wk) at near term-equivalent age, without administration of sedation or intravenous contrast. Images were scored by a radiologist using a modified Ochiai score, and volumes of high- and low-signal intensity lung parenchyma were quantified by segmentation and threshold analysis.

Measurements and Main Results: Signal increases, putatively combinations of fibrosis, edema, and atelectasis, were present in all premature infants. Infants with diagnosed BPD had significantly greater volume of high-signal lung (mean ± SD, 26.1 ± 13.8%) compared with full-term infants (7.3 ± 8.2%; $P = 0.020$) and premature infants without BPD (8.2 ± 6.4%; $P = 0.026$). Signal decreases, presumably alveolar simplification, only appeared in the most severe BPD cases, although cystic appearance did increase with severity.

Conclusions: Pulmonary MRI reveals quantifiable, significant differences between patients with BPD, premature patients without BPD, and full-term control subjects. These methods could be implemented to individually phenotype disease, which may impact clinical care and predict future outcomes.

Keywords: bronchopulmonary dysplasia; magnetic resonance imaging; prematurity; NICU

Very low birth weight (<1,500 g) and low gestational age (GA; gestational age is defined as the number of weeks from the beginning of the last menstrual period [approximately 2 wk prefertilization] to birth) infants represent a small fraction of live births in the United States but a disproportionately high percentage of newborn healthcare costs. These neonates are susceptible to myriad pulmonary complications that require longer durations of stay in the neonatal intensive care unit (NICU) and additional clinical resources (1). The most common respiratory complication of preterm birth, bronchopulmonary dysplasia (BPD), defined by a clinically assessed need for supplemental oxygen support at 36 weeks post-menstrual age (2), has actually increased in incidence as advancements in clinical respiratory care (i.e., implementation of less-aggressive ventilation strategies, steroid and surfactant therapies) have improved initial survivability for very premature neonates.

For many patients, however, the burden of pulmonary disease continues

(Received in original form March 19, 2015; accepted in final form July 16, 2015)

Supported by National Institutes of Health grant T32 HL007752 and The Perinatal Institute at Cincinnati Children's Hospital Medical Center.

Author Contributions: Concept and design, L.L.W., J.A.T., N.S.H., R.P.T., S.B.F., and J.C.W. Analysis and interpretation, L.L.W., J.A.T., N.S.H., R.P.T., S.B.F., S.L.M., R.J.F., R.S.A., and J.C.W. All authors contributed to the intellectual content of the manuscript.

Correspondence and requests for reprints should be addressed to Jason C. Woods, Ph.D., Cincinnati Children's Hospital Medical Center, Center for Pulmonary Imaging Research, 3333 Burnet Avenue, Cincinnati, OH 45229. E-mail: jason.woods@cchmc.org

Am J Respir Crit Care Med Vol 192, Iss 10, pp 1215–1222, Nov 15, 2015

Originally Published in Press as DOI: 10.1164/rccm.201503-0552OC on July 17, 2015
Internet address: www.atsjournals.org

At a Glance Commentary

Scientific Knowledge on the Subject: Bronchopulmonary dysplasia is a common respiratory complication of premature birth and is essentially defined by an oxygen dependence; very little is known about the underlying structural pathologies. Survivors (particularly those of very low birth weight and/or gestational age) are at higher risk for respiratory complications and morbidity with unclear linkages between initial clinical diagnosis and long-term outcomes.

What This Study Adds to the Field: This study demonstrates that pulmonary magnetic resonance imaging can be performed safely and successfully in the neonatal intensive care unit environment and that multiple underlying structural abnormalities exist in patients with bronchopulmonary dysplasia compared with full-term control subjects. These results support wider implementation of magnetic resonance imaging as a safe, nonionizing tool for longitudinal assessment of the lungs of very young children.

beyond the NICU; these survivors are at greater risk for respiratory-related rehospitalization and diminished pulmonary capacity, and methods for longitudinal assessment and prediction of outcomes are lacking in this population (2–7).

Pulmonary imaging of the neonate has been limited to the clinical assessment of acute changes in respiratory status. The most widely accessible clinical imaging modalities, radiograph and computed tomography (CT), have significant limitations (8, 9). Although chest radiograph is routine for acute assessment, the technique's sensitivity is limited because patients with significant respiratory dysfunction may exhibit only minor radiographic abnormalities (10–12), and although CT is considered the gold standard for clinical pulmonary imaging, it is not widely implemented because neonates may require sedation, especially for high-resolution CT, and are especially vulnerable to damage from ionizing radiation (13, 14). Furthermore, CT is not appropriate for longitudinal assessment because of the link between serial radiation exposure and increased cancer risk (4).

As a nonionizing technique, magnetic resonance imaging (MRI) is superficially an ideal modality for pulmonary imaging; nevertheless, MRI has played a limited role because of technologic challenges: the low ^{1}H density of the lung parenchyma (only ~20% that of solid tissues), numerous air-tissue interfaces that lead to rapid signal decay (i.e., short T_2^*, ~2 ms at 1.5 T [15]), and cardiac and respiratory sources of motion that further degrade image quality (16). Pulmonary MRI of the neonate is additionally confounded by small patient size and the delicate nature of transporting a NICU patient to the scanner. To overcome the latter two challenges, we extend the application of a unique, small footprint 1.5-T MRI scanner designed by our colleagues in the Imaging Research Center at Cincinnati Children's Hospital for installation and clinical use in our NICU (17–19) to image neonatal lungs. Using this scanner, commercial MRI sequences, and quantitative analysis, we demonstrate the ability of MRI to spatially map and quantify lung pathology associated with premature birth in quietly breathing neonates. Some of these results have been previously reported in the form of abstracts (20, 21).

Methods

NICU MRI Patient Cohort

After institutional review board approval, patients were recruited from our NICU and parental consent was obtained. Eighteen patients (Table 1) were enrolled and divided into three subgroups: a full-term control group (n = 6), defined as NICU patients born at greater than or equal to 36 weeks GA without major, suspected pulmonary complications; a premature non-BPD group (n = 6), defined as birth at less than 36 weeks GA without a BPD diagnosis; and a BPD group (n = 6), defined as premature infants with a clinical diagnosis of BPD. Subjects Term3, Term4, and Term5 were imaged before surgery; Term1 and Term6 were imaged 2 weeks post-surgery, and Term2 was imaged 3 weeks post-surgery.

Image Acquisition

A small-footprint 1.5-T orthopedic MRI scanner (ONI Medical Systems, currently GE Healthcare, Waukesha, WI) was previously adapted for clinical use in our NICU (17–19); the scanner's 18-cm bore can accommodate infants weighting up to approximately 4,000 g. Using this scanner, standard axial three-dimensional fast gradient echo (FGRE) images were acquired in all 18 patients (repetition time/echo time [TR/TE] ~7/1.9 ms; 10° flip angle; 18–20 cm field of view; 3 mm slice thickness; 5–10 averages). Additionally, fast spin echo (FrFSE) images were acquired for 10 patients (TR/TE 3,000/11.6 ms; 16 cm field of view; 3 mm slice thickness; echo train length 5) and Propeller images (TR/TE 3,750/32.5 ms; 16 cm field of view; 3 mm slice thickness; echo train length 10) were acquired for 11 patients. Patients were fed, swaddled, and equipped with ear protection directly before imaging. Subjects were imaged during quiet breathing; all full-term control subjects, all premature non-BPD patients (except Premature2), and BPD4 were imaged while freely breathing room air; Premature2, BPD1, BPD3, BPD5, and BPD6 were supported by O_2 via nasal cannula, and BPD2 was mechanically ventilated during the study (positive end-expiratory pressure, 7 cm H_2O; 40 breaths per min). No intravenous contrast agent or sedation was administered as part of the study; preimaging preparation and total scanner time was about 1 hour, with approximately 30 minutes for image localization and acquisition. For comparison with the MRIs, clinical chest radiograph films for all patients (dated closest to the MRI examination) and clinically ordered CT images for two patients (BPD1 and BPD2) were obtained from medical records.

Quantification and Analysis

MRIs were clinically scored by a radiologist with no prior knowledge of clinical diagnosis using a modified Ochiai scoring system (Table 2) with a higher score reflective of more severe findings (range, 0–14) (22); the radiologist also scored the diagnostic quality of the images (0–2, with 0 considered nondiagnostic quality). Quantitative image analysis was performed using ImageJ (23) and Amira (FEI Visualization Sciences Group, Hillsboro, OR). Parenchymal signal-to-noise and signal-to-muscle ratios were measured for multiple regions of interest in equivalent anatomic regions of the lung across several slices per patient. For

Table 1. Cohort of NICU Patients

Patient ID (Diagnosis)	Birth GA (*wk*)	Birth Mass (*g*)	Sex	PMA at MRI (*wk*)	Day of Life at MRI (*d*)	Mass at MRI (*g*)	Total Days on Respiratory Support until Discharge: Type (*d*)
Full-term group (n = 6)							
Term1 (gastroschisis)	36	3,145	F	38	14	3,500	13: NIV (1)/NC (12)
Term2 (gastroschisis)	36	2,807	F	40	27	3,200	5: MV (5)
Term3 (spinal dysraphism)	37	2,920	F	38	12	3,000	0: RA
Term4 (anorectal malformation)	38	3,590	M	38	2	4,000	0: RA
Term5 (tethered cord)	39	3,160	F	39	2	3,060	0: RA
Term6 (Hirschsprung disease)	39	2,619	F	41	14	2,640	0: RA
Premature (non-BPD) group (n = 6)							
Premature1	34	1,900	F	35	6	1,830	4: NC (4)
Premature2	34	2,370	M	35	6	2,170	6: NC (6)
Premature3	32	1,860	F	37	39	2,630	0: RA
Premature4	35	2,380	F	37	15	2,370	0: RA
Premature5	29	1,490	M	36	41	2,680	32: NIV (12)/NC (20)
Premature6	34	2,466	F	38	28	2,500	6: NC (6)
BPD group (n = 6)							
BPD1	23	595	M	39	111	3,000	130: MV (56)/NIV (50)/NC (24) transferred on NC
BPD2	26	1,000	M	39	89	3,500	247: MV (247) discharged on home ventilator
BPD3	27	1,060	M	35	67	2,800	83: MV (22)/NIV (14)/NC (47) discharged on O_2
BPD4	28	1,120	M	40	83	3,700	43: MV (2)/NIV (41) transferred on NIV
BPD5	28	1,390	M	36	77	4,000	75: MV (35)/NC (40) discharged on O_2
BPD6	29	1,090	F	37	61	2,300	84: MV (25)/NIV (7)/NC (52) discharged on O_2

Definition of abbreviations: BPD = bronchopulmonary dysplasia; GA = gestational age; MRI = magnetic resonance imaging; MV = mechanical ventilation; NC = nasal cannula; NICU = neonatal intensive care unit; NIV = noninvasive ventilation; PMA = post-menstrual age; RA = room air.

segmentation analysis of the FGRE images, separate masks were generated for the chest soft tissue (excluding the lungs) and the lung parenchyma (excluding major airways and vasculature). Mean signal intensities for the chest and lung masks were calculated, and the signal from the lung was normalized to the mean chest soft tissue. Masks of high- and low-signal intensity parenchyma were obtained by thresholding the MRI signal intensity. High-signal regions of the lung parenchyma (i.e., regions of potential fibrosis, bronchiectasis, edema, and/or atelectasis) were segmented by thresholding pixels with intensity greater than 45% of the mean chest soft tissue signal; likewise, low-signal lung parenchyma (i.e., regions of suspected alveolar simplification) was segmented by thresholding pixels with signal intensity less than 4% of the mean chest soft tissue signal. These thresholds were chosen empirically based on visual appearance to maximize contrast among groups. Volume percentages were calculated to determine the amount of affected lung. Mean and SD of high- and low-signal volume percentages were calculated for each subcohort, and a two-tailed Student *t* test with unequal variance was performed to determine statistical significance (defined as $P \leqslant 0.05$) among groups.

Table 2. Radiologic Scoring System for Pulmonary MRI of NICU Patients

Category	Scoring		
	0	1	2
Hyperexpansion	None	Focal	Global
Mosaic lung attenuation	None	Unclear	Obvious
Emphysema, number of cysts/regions	None	Single	Multiple
Emphysema, size	None	<5 mm	>5 mm
Fibrous/interstitial, triangular subpleural opacities	None	1–3 lobes	4–6 lobes
Distortion of bronchovascular bundles	Mild	Moderate	Severe
Subjective impression	Mild	Moderate	Severe

Definition of abbreviations: MRI = magnetic resonance imaging; NICU = neonatal intensive care unit.

Results

The protocol was well tolerated by the patients; most of the infants did not stir during imaging, and for the few that did, the scanner was paused and the patient was soothed for a few minutes before continuing. The resulting images obtained were of high-diagnostic quality (mean quality score, 1.65) and relatively free from respiratory and cardiac motion artifacts. Radiologic scoring of the MRIs using the

system in Table 2 showed significantly higher scores in the BPD group (7.7 ± 4.5, mean ± SD) compared with the full-term group (0.17 ± 0.41; $P = 0.009$) and compared with the premature group (2.8 ± 2.1; $P = 0.046$). Also, the premature group had significantly higher clinical scores than the full-term group ($P = 0.027$).

Table 3 summarizes the quantitative volumetric thresholding analysis for the FGRE images. Images of the prematurely-born infants revealed more high-intensity parenchyma than full-term control subjects, with the most striking differences found in BPD patients. BPD patients had a significantly higher volume percentage of high-signal intensity lung (26.1 ± 13.8%) compared with the premature group (8.2 ± 6.4%; $P = 0.026$) and compared with the full-term group (7.3 ± 8.2%; $P = 0.020$). There was no significant difference in the high-signal analysis between the premature and full-term groups ($P = 0.83$). For the low-signal intensity analysis (our quantitative measure of alveolar simplification), there was no significant difference between the BPD group (0.55 ± 0.55%) and the full-term group (1.4 ± 1.8%; $P = 0.33$) or premature group (0.9 ± 1.2%; $P = 0.49$), nor was the difference between the premature and full-term groups significant ($P = 0.62$).

The parenchymal appearance of BPD varied widely among patients, with most exhibiting heterogeneous structure with a few dispersed pockets of relatively lower signal intensity (presumably alveolar simplification) and others with more uniformly elevated parenchymal signal throughout. Figure 1 compares FGRE images with clinical chest radiographs for a premature patient without BPD and three BPD patients. Radiologic reads of BPD patient chest films included diffuse and reticular opacities consistent with edema and/or atelectasis. Compared with radiograph, MRI more clearly shows the differences in parenchymal structure between the BPD patients and also between BPD and non-BPD premature patients. Elements of mosaic attenuation and fibrotic opacities are observed in the MRIs for patient BPD5; for subjects BPD3 and BPD2, these features and multiple regions of emphysema (i.e., alveolar simplification) and hyperexpansion are described in the clinical reads.

Figure 2 is an example of the quantitative volumetric segmentation of high-intensity and low-density parenchyma for FGRE images from a full-term control patient, a non-BPD premature patient, and two BPD patients. The high-signal intensity mask identifies all high-density abnormalities, likely representing combinations of edema, atelectasis, fibrosis, and bronchiectasis, whereas the low-signal threshold identifies potential regions of alveolar simplification and gas trapping (low-density parenchyma). Interestingly, the results from Figure 2 are representative of the groups, in that alveolar simplification was identified only in the most severe BPD cases (e.g., BPD2).

Figure 3 compares the FGRE, FrFSE, and Propeller pulse sequences in control subject Term4 and in BPD patient BPD3. All three sequences capture elements of the parenchymal signal in the full-term control patient: the parenchyma-to-muscle signal ratios (mean ± SD) are 0.13 ± 0.02, 0.39 ± 0.09, and 0.33 ± 0.09 for the FGRE, FrFSE, and Propeller images, respectively. The parenchyma of BPD3 in Figure 3 is more heterogeneous with diffuse regions of increased signal intensity relative to the control patient; the BPD parenchymal-to-muscle signal ratios are 0.31 ± 0.16, 0.57 ± 0.14, and 0.54 ± 0.18 for the FGRE, FrFSE, and Propeller images, respectively.

The FGRE images, which were proton density– and T_2*-weighted, provided the most consistent contrast between lung parenchyma and vasculature and sufficient signal intensity for quantification. Although parenchymal signal is more intense in the FrFSE images, detail in the vasculature and pathology is killed, and the sequence is more susceptible to motion as evidenced by the artifacts in the images. The Propeller sequence has similar signal-to-noise as FrFSE but is more robust to motion artifacts (better demonstrated in BPD3) (Figure 3). Regions of increased parenchymal signal were common in all premature patients, and the structural differences between the full-term and BPD patient are most striking and best resolved in the FGRE images because of better contrast from the increased proton density and long T_2* components of disease.

For patient BPD1, a clinically ordered chest CT was performed the day before MRI, which provided a unique opportunity for direct comparison of the modalities (Figure 4). A clinical chest radiograph taken 4 days before the MRI study is also included. Although the CT and FGRE MRIs differ in resolution ($0.29 \times 0.29 \times 3$ mm^3 and $0.78 \times 0.78 \times 3$ mm^3, respectively), strikingly similar lung architecture with regions of increased and decreased density throughout the parenchyma is revealed, and clinical reads include the same pathologic features (i.e., focal hyperexpansion, emphysema, diffuse and fibrous opacities, and bronchovascular distortion).

Discussion

We demonstrate diagnostic-quality, quantitative pulmonary MRI in neonates using a small-footprint 1.5-T scanner within our NICU and standard commercial pulse sequences. Although wider implementation of MRI scanners in NICUs is on the horizon, the pulse sequences and quantitative methods presented here are readily

Table 3. Summary of Radiologic Score and Quantitative Analysis of FGRE Images

Group	Radiologic Score	Normalized Parenchymal Signal Intensity	Percentage High-Signal Lung Parenchyma	Percentage Low-Signal Lung Parenchyma
Full-term	0.17 ± 0.41 (0–1)	0.26 ± 0.07 (0.15–0.35)	7.3 ± 8.2 (0–18.1)	1.4 ± 1.8 (0.1–4.9)
Premature, non-BPD	2.8 ± 2.1 (0–5)	0.27 ± 0.05 (0.19–0.33)	8.2 ± 6.4 (1.0–19.8)	0.9 ± 1.2 (0.2–3.4)
BPD	7.7 ± 4.5 (1–14)	0.36 ± 0.07 (0.25–0.46)	26.1 ± 13.8 (5.3–40.9)	0.6 ± 0.6 (0–1.3)

Definition of abbreviations: BPD = bronchopulmonary dysplasia; FGRE = fast gradient echo.
Data are mean ± SD (range).

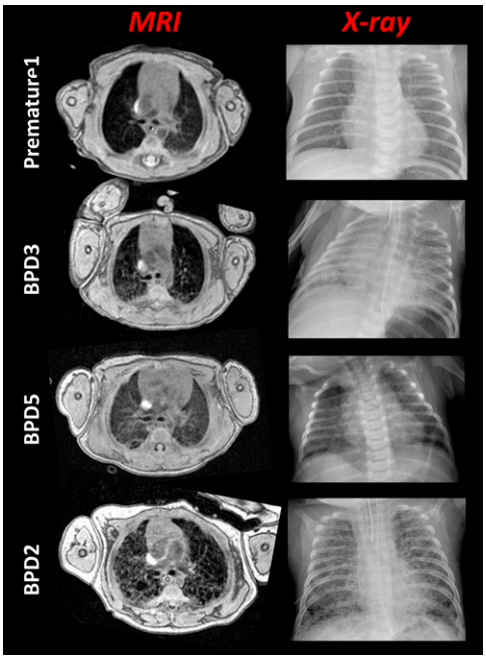

Figure 1. Phenotyping lung disease in neonates with quantitative magnetic resonance imaging (MRI). For each patient, an axial fast gradient echo slice (taken near the carina) is compared with a clinical chest radiograph. Notice the vastly differing parenchymal structure in each of the patients. Day of chest radiograph (MRI date as Day 0): Premature1 (Day −5), BPD3 (Day −17), BPD5 (Day −2), and BPD2 (Day +2). The radiologic scores for the MRIs were 2, 10, 5, and 14 for Premature1, BPD3, BPD5, and BPD2, respectively, using the system in Table 2. BPD = bronchopulmonary dysplasia.

accessible and could be deployed on a conventional adult-sized scanner using coils appropriately sized for the neonate, thus providing a routine, nonionizing means of imaging the lung parenchyma and vasculature. The images are relatively free from significant motion artifacts as determined by the radiologist, with the exception of some respiratory ghosting in the FrFSE images. The proton density– and T_2*-weighted contrast in the FGRE MRI best emphasized the structural differences between the groups, and BPD patients had significantly higher radiologic scores and volume percentages of high-signal intensity parenchyma as compared with full-term control subjects and premature peers without BPD. Interestingly, although radiologic scoring for the most severe BPD cases included emphysema or alveolar simplification, this is not reflected in the low-signal quantitative analysis of the FGRE images. This suggests that although the cystic appearance of the lungs increases with BPD severity, the pockets of relatively darker parenchyma have signal intensities consistent with lung parenchyma of full-term control patients.

Even in this relatively small cohort, using radiologic scoring and quantitative analysis, MRI can differentiate BPD patients from premature infants without BPD. The increased parenchymal signal intensity in premature (non-BPD) patients is likely from lung fluid or edema as opposed to fibrotic pathologies observed in BPD. Fetal lung fluid plays a vital role in lung development, and in preparation for the transition to air breathing *ex utero*, secretion of fetal lung fluid declines in the days before labor. Infants born prematurely are estimated to have approximately 25% greater lung water content than full-term peers (24); this likely contributes to increased parenchymal fluid and the increased signal intensity observed in the MRIs of premature infants, although it can be in addition to other factors including immature surfactant production and decreased activity of epithelial sodium channels (responsible for lung fluid absorption). The increased lung fluid observed in these premature patients weeks and months after birth may be reflective of persistent fluid-handling abnormalities and/or disease.

Importantly, in the BPD group, high-signal intensity (arising from increased proton density and lengthened T_2*) is more concentrated in fibrotic opacities and bronchovascular bundling as opposed to diffusely distributed throughout the parenchyma. Furthermore, a cystic appearance of the parenchyma is observed only in the BPD group and is entirely absent in both the premature patients without BPD and the full-term control subjects. This cystic appearance presumably would be caused by alveolar simplification (emphysema), although quantitative analysis for low-signal intensity did not show a significant difference among groups. Increasing the threshold to less than 5% or less than 10% of the mean chest soft tissue signal did not increase group separation (using a $<$10% threshold, the mean $\pm$ SD volume percentages for the groups were 3.9 $\pm$ 3.4%, 6.6 $\pm$ 6.6%, and 8.8 $\pm$ 9.8% for the BPD, premature, and full-term groups, respectively; $P \geq 0.3$ for any group comparison).

It is possible that our quantitative MRI analysis fails to include areas of alveolar simplification that would be identified by clinical reads. For example, three of the BPD subjects showed at least minor evidence of cystic appearance, but the MRI signal intensity within these cysts was consistent with the parenchymal signal measured in the full-term control subjects. Notably, these cystic areas had slightly reduced radiographic attenuation in the two BPD cases where clinical CT images were available for comparison (approximately −870 HU), which suggests some alveolar simplification. This small discrepancy between CT and MRI likely results from the lower resolution of MRI (and edge-blurring at the thick sepal walls bounding the cystic areas) compared with CT. We expect that increased MRI resolution will reduce these areas of CT-MRI disagreement, particularly with newer ultrashort echo time (UTE) sequences (25, 26).

Although no sedation was administered during this research protocol, in one case (Term5), midazolam (Versed) had been administered (oral, 0.5 mg/kg dose) approximately 2 hours before our study to aid quiescence for a clinically ordered MRI examination. Even still, this is a significant improvement over the general anesthesia needed for CT protocols using inspiratory and expiratory phase imaging in neonates and young children (27). Although the MRIs are not as high resolution as CT, the risks of anesthesia and ionizing radiation must be considered in the particularly vulnerable NICU

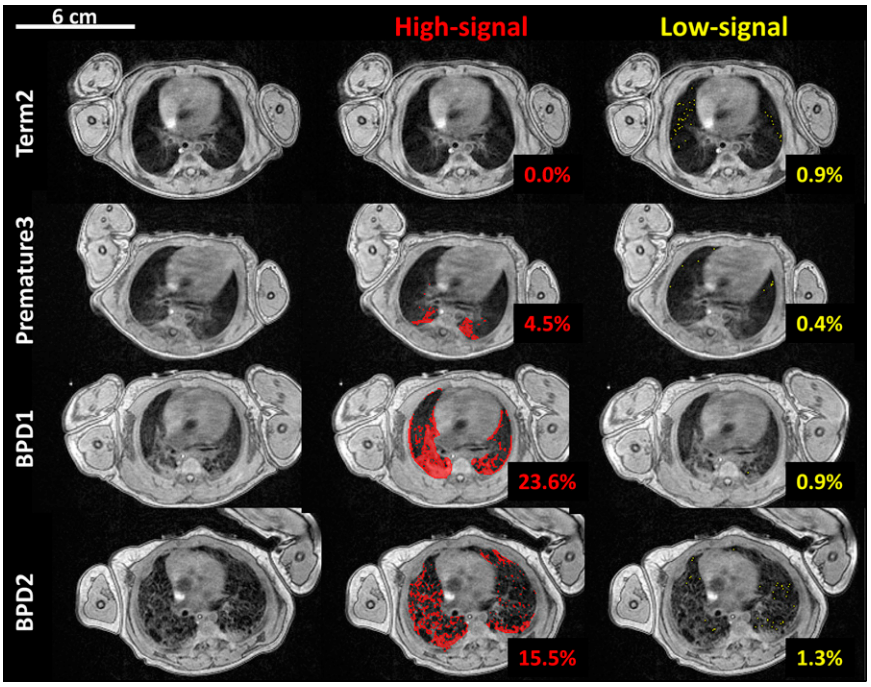

Figure 2. Fast gradient echo image segmentation of high- and low-signal intensity parenchyma in four neonatal intensive care unit patients (*top to bottom*): a full-term control subject (Term2), a premature patient (Premature3), and two bronchopulmonary dysplasia (BPD) patients (BPD1 and BPD2). The first column is a representative axial slice near the hilum without masking. High-signal (defined as pixels >45% of the mean chest soft tissue signal) and low-signal (<4% of the mean chest soft tissue signal) lung parenchyma are indicated in *red* and *yellow*, *middle* and *right columns*, respectively. The volume percentages of the thresholded pixels for the whole-lung analysis are included.

population. Moreover, the similarity of the fundamental structures on CT and MRI when compared with Figure 4 suggest that MRI can be a viable approach for detecting major lung abnormalities despite the reduced spatial resolution. The radiologic scoring of the CT and MR images in Figure 4 were 12 and 9, respectively, and the differences in scoring were in the emphysema ("single region of >5 mm size" in CT vs. "multiple regions of <5 mm" in MRI), distortion of bronchovascular bundles ("severe" in CT, "moderate" in MRI), and subjective impression ("severe" in CT, "moderate" in MRI) categories. The much larger regions of confluent opacity in the CT images are likely atelectasis caused by the patient being anesthetized during that procedure, and we emphasize that no anesthesia was required for the MRI. In the two patients for whom these direct comparisons between modalities could be made, very good agreement between the parenchymal structural features and radiologic scoring was achieved, suggesting the risk-benefit may favor MRI over CT.

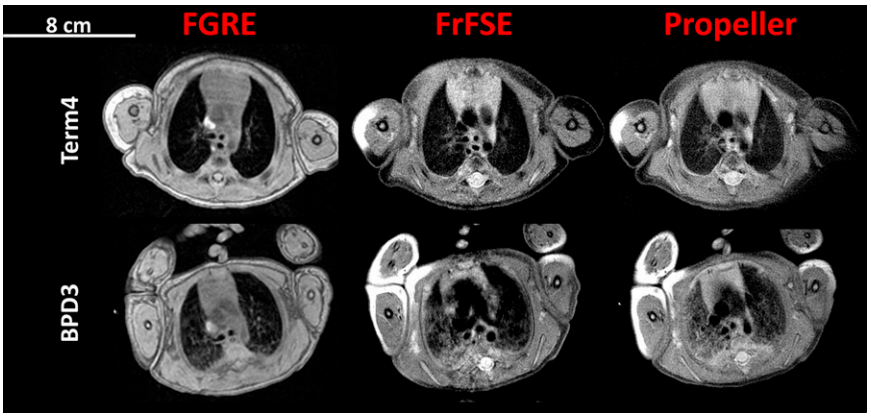

Figure 3. Axial slices near the carina of a full-term control subject (Term4) and bronchopulmonary dysplasia (BPD) patient (BPD3) (*top* and *bottom rows*, respectively) demonstrating the fast gradient echo (FGRE), fast spin echo (FrFSE), and Propeller pulse sequences. Although the fast spin echo sequences (FrFSE and Propeller) show increased parenchymal signal intensity, the proton density–and T_2*-weighted FGRE images provided the most consistent contrast between the BPD and full-term patients. Here, BPD parenchymal signal-to-muscle signal ratios were elevated by a factor of 2.4 in the FGRE images (see RESULTS).

Our results are in good agreement with work from Adams and colleagues (28) at Hammersmith Hospital (London, UK), who reported heterogeneously distributed regions of increased lung density in NICU patients with BPD. Increased density in the dependent regions of the lung may be atelectasis or increased lung fluid, and in their study, imaging the patient supine and prone (when appropriate) confirmed the presence of lung fluid (29). They report that the lungs of premature infants had a higher relative proton density compared with full-term peers, which is consistent with our findings. However, our study differs in several ways; we use a small-footprint 1.5-T MRI scanner and implement a FGRE pulse sequence with a shorter echo time, shorter repetition time, and a lower flip angle for faster imaging and whole-lung volumetric quantification of the parenchyma. Our scoring system takes into account different types of high-signal intensity pathologies, and we objectively quantify proton density of the parenchyma.

Our study is not without limitations. In this small cohort, the BPD infants were significantly smaller at birth than their peers without BPD; the mean ± SD birth weight for the BPD group was 1,042 ± 257 g, compared with 2,078 ± 388 g for the premature non-BPD group and 3,040 ± 339 g for the full-term group. As expected, the BPD group was also born at a significantly lower GA than the premature (non-BPD) and full-term groups; the mean ± SD GA for the BPD group was 26.8 ± 2.1 weeks, compared with 33 ± 2.2 weeks for the premature group and 37.5 ± 1.4 weeks for the full-term group.

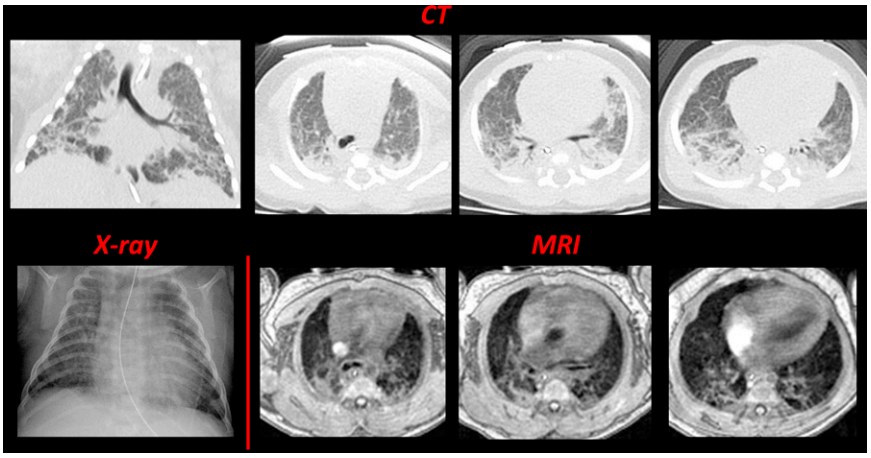

Figure 4. Comparing computed tomography (CT), radiograph, and magnetic resonance imaging (MRI) in a neonatal intensive care unit patient diagnosed with bronchopulmonary dysplasia (BPD) (BPD1, 23-wk gestational age at birth). The *top* contains four inspiratory CT images (clinically ordered; 80 kVp; 500 ms exposure), one representative coronal slice (*left*) and three axial slices, which were selected to best match the three fast gradient echo MRI images in the *bottom*. The chest radiograph (*bottom left*) is also included for comparison. CT and chest radiograph images were acquired at Day −1 and Day −4, respectively, relative to MRI acquisition (Day 0). The radiologic scores (Table 2) were 12 and 9, respectively for the CT and MRIs.

At the time of MRI, the full-term group was significantly larger than the premature non-BPD group (3,233 ± 468 g vs. 2,363 ± 320 g, respectively; $P = 0.005$) but not significantly larger than the BPD group (3,217 ± 631 g). In future studies, BPD subjects will be matched for GA and/or birth weight with premature infants without BPD.

The FGRE MR images are not corrected for T_1, T_2, or T_2* decay, but assuming both soft tissue and lung parenchyma have similar T_1 and T_2 (∼1,000 ms and 40 ms, respectively, at 1.5 T [16]) and operating in a low flip angle regime (∼10°), it is reasonable to assume that the FGRE images (normalized to the mean soft tissue chest signal) are only proton density– and T_2*-weighted. Imaging with a lower flip angle (i.e., 3–4°) is an additional improvement, which we are currently implementing. Although it increases objectivity and potential efficiency, one drawback of the quantitative thresholding analysis is that it is incapable of distinguishing different pathologies from one another (e.g., fibrosis vs. atelectasis). In the future, the quantitative and textural differentiation of high-intensity pathologies will be explored; we hypothesize that the macromolecular structural differences of these pathologies will give rise to differential relaxation and/or textural properties, and that information will be used to refine the quantitative threshold analysis. In addition to these efforts, we are adapting other pulmonary imaging methods, including UTE (25, 26) and hyperpolarized-gas MRI (30) techniques for neonatal patients. We expect that in the future, UTE MRI will provide higher spatial resolution and some insensitivity to motion artifacts and that hyperpolarized-gas MRI will illuminate regional pulmonary function and airspace size.

In concert, these MRI methods will provide spatially resolved quantification of the macrostructural and microstructural and functional relationships in the neonatal lung. Although hyperpolarized-gas MRI currently is limited to specialized research centers, the methods in this study rely on standard product pulse sequences and with refinement could be implemented for neonatal lung imaging on adult-sized scanners.

Much of what is known about BPD has been revealed through biopsy and post-mortem studies, which may have skewed the pathologic perception of this condition toward more severe cases. As we demonstrate, quantitative MRI has the potential to reexamine and refine the definitions of BPD, to move beyond grading the condition by its treatment and instead focus on individual pathologic characteristics; in particular, there is great opportunity for MRI to describe very mild and moderate BPD where pathologic descriptions are less clear than those for severe BPD. Furthermore, quantitative pulmonary MRI can be implemented serially from early life and serve as a foundation for longitudinal assessment, objectively measuring changes in the lung parenchyma as these patients age, and can be compared with pulmonary function tests as survivors grow. Indeed, there is evidence of "catch-up alveolarization" in formerly premature school-age children from hyperpolarized ^{3}He MRI (31, 32). In cases of acquired lobar emphysema, a rare but significant consequence of severe BPD sometimes requiring pneumonectomy, quantitative MRI of the lung parenchyma could provide an additional means of presurgical and post-surgical assessment (33). Also, in congenital abnormalities, such as congenital diaphragmatic hernia, there is opportunity for these methods to monitor catch-up and/or compensatory lung growth. With further refinement, quantitative pulmonary MRI methods may be able to recognize the structural phenotypes contributing to an individual patient's condition, and in the future may inform therapy, monitor treatment efficacy, and assess postnatal lung growth and development. ■

Author disclosures are available with the text of this article at www.atsjournals.org.

References

1. Johnson TJ, Patel AL, Jegier BJ, Engstrom JL, Meier PP. Cost of morbidities in very low birth weight infants. *J Pediatr* 2013;162: 243–249.e1.
2. Jobe AH. The new bronchopulmonary dysplasia. *Curr Opin Pediatr* 2011; 23:167–172.
3. Ghanta S, Leeman KT, Christou H. An update on pharmacologic approaches to bronchopulmonary dysplasia. *Semin Perinatol* 2013;37:115–123.
4. Bhandari A, McGrath-Morrow S. Long-term pulmonary outcomes of patients with bronchopulmonary dysplasia. *Semin Perinatol* 2013;37: 132–137.
5. Gibson AM, Doyle LW. Respiratory outcomes for the tiniest or most immature infants. *Semin Fetal Neonatal Med* 2014;19:105–111.

6. Stoll BJ, Hansen NI, Bell EF, Shankaran S, Laptook AR, Walsh MC, Hale EC, Newman NS, Schibler K, Carlo WA, *et al*.; Eunice Kennedy Shriver National Institute of Child Health and Human Development Neonatal Research Network. Neonatal outcomes of extremely preterm infants from the NICHD Neonatal Research Network. *Pediatrics* 2010;126: 443–456.
7. Simpson SJ, Hall GL, Wilson AC. Lung function following very preterm birth in the era of "new" bronchopulmonary dysplasia. *Respirology* (In press)
8. Wilson AC. What does imaging the chest tell us about bronchopulmonary dysplasia? *Paediatr Respir Rev* 2010;11:158–161.
9. Rossi UG, Owens CM. The radiology of chronic lung disease in children. *Arch Dis Child* 2005;90:601–607.
10. Breysem L, Smet MH, Van Lierde S, Devlieger H, De Boeck K. Bronchopulmonary dysplasia: correlation of radiographic and clinical findings. *Pediatr Radiol* 1997;27:642–646.
11. Oppenheim C, Mamou-Mani T, Sayegh N, de Blic J, Scheinmann P, Lallemand D. Bronchopulmonary dysplasia: value of CT in identifying pulmonary sequelae. *AJR Am J Roentgenol* 1994;163:169–172.
12. Toce SS, Farrell PM, Leavitt LA, Samuels DP, Edwards DK. Clinical and roentgenographic scoring systems for assessing bronchopulmonary dysplasia. *Am J Dis Child* 1984;138:581–585.
13. Brenner D, Elliston C, Hall E, Berdon W. Estimated risks of radiation-induced fatal cancer from pediatric CT. *AJR Am J Roentgenol* 2001;176:289–296.
14. Pearce MS, Salotti JA, Little MP, McHugh K, Lee C, Kim KP, Howe NL, Ronckers CM, Rajaraman P, Sir Craft AW, *et al*. Radiation exposure from CT scans in childhood and subsequent risk of leukaemia and brain tumours: a retrospective cohort study. *Lancet* 2012;380:499–505.
15. Yu J, Xue Y, Song HK. Comparison of lung T2* during free-breathing at 1.5 T and 3.0 T with ultrashort echo time imaging. *Magn Reson Med* 2011;66:248–254.
16. Mulkern R, Haker S, Mamata H, Lee E, Mitsouras D, Oshio K, Balasubramanian M, Hatabu H. Lung Parenchymal signal intensity in MRI: a technical review with educational aspirations regarding reversible versus irreversible transverse relaxation effects in common pulse sequences. *Concepts Magn Reson Part A Bridg Educ Res* 2014;43a:29–53. (PubMed).
17. Tkach JA, Hillman NH, Jobe AH, Loew W, Pratt RG, Daniels BR, Kallapur SG, Kline-Fath BM, Merhar SL, Giaquinto RO, *et al*. An MRI system for imaging neonates in the NICU: initial feasibility study. *Pediatr Radiol* 2012;42:1347–1356.
18. Tkach JA, Merhar SL, Kline-Fath BM, Pratt RG, Loew WM, Daniels BR, Giaquinto RO, Rattan MS, Jones BV, Taylor MD, *et al*. MRI in the neonatal ICU: initial experience using a small-footprint 1.5-T system. *AJR Am J Roentgenol* 2014;202:W95–W105.
19. Tkach JA, Li Y, Pratt RG, Baroch KA, Loew W, Daniels BR, Giaquinto RO, Merhar SL, Kline-Fath BM, Dumoulin CL. Characterization of acoustic noise in a neonatal intensive care unit MRI system. *Pediatr Radiol* 2014;44:1011–1019.
20. Walkup LL, Tkach JA, Nar SH, Merhar S, Cao X, Thomen RP, Amin R, Fain SB, Woods JC. MRI Characterization of bronchopulmonary dysplasia in the NICU: preliminary results [abstract]. *Am J Respir Crit Care Med* 2015;191:A5131.
21. Walkup LL, Tkach JA, Thomen RP, Merhar SL, Amin R, Kingma P, Woods JC. Pulmonary MRI in the NICU: initial experience imaging BPD and CDH with a small-footprint scanner. Presented at the Radiological Society of North America 2014 Scientific Assembly and Annual Meeting. November 30 to December 5, 2014, Chicago, IL.
22. Ochiai M, Hikino S, Yabuuchi H, Nakayama H, Sato K, Ohga S, Hara T. A new scoring system for computed tomography of the chest for assessing the clinical status of bronchopulmonary dysplasia. *J Pediatr* 2008;152:90–95.e3.
23. Schneider CA, Rasband WS, Eliceiri KW. NIH Image to ImageJ: 25 years of image analysis. *Nat Methods* 2012;9:671–675.
24. Katz C, Bentur L, Elias N. Clinical implication of lung fluid balance in the perinatal period. *J Perinatol* 2011;31:230–235.
25. Johnson KM, Fain SB, Schiebler ML, Nagle S. Optimized 3D ultrashort echo time pulmonary MRI. *Magn Reson Med* 2013;70:1241–1250.
26. Molinari F, Madhuranthakam AJ, Lenkinski R, Bankier AA. Ultrashort echo time MRI of pulmonary water content: assessment in a sponge phantom at 1.5 and 3.0 Tesla. *Diagn Interv Radiol (Ank)* 2014;20:34–41.
27. Mahmoud M, Towe C, Fleck RJ. CT chest under general anesthesia: pulmonary, anesthetic and radiologic dilemmas. *Pediatr Radiol* 2015; 45:977–981.
28. Adams EW, Harrison MC, Counsell SJ, Allsop JM, Kennea NL, Hajnal JV, Thornton AS, Duggan P, Edwards AD. Increased lung water and tissue damage in bronchopulmonary dysplasia. *J Pediatr* 2004;145: 503–507.
29. Adams EW, Counsell SJ, Hajnal JV, Cox PN, Kennea NL, Thornton AS, Bryan AC, Edwards AD. Magnetic resonance imaging of lung water content and distribution in term and preterm infants. *Am J Respir Crit Care Med* 2002;166:397–402.
30. Walkup LL, Woods JC. Translational applications of hyperpolarized 3He and 129Xe. *NMR Biomed* 2014;27:1429–1438.
31. Narayanan M, Beardsmore CS, Owers-Bradley J, Dogaru CM, Mada M, Ball I, Garipov RR, Kuehni CE, Spycher BD, Silverman M. Catch-up alveolarization in ex-preterm children: evidence from (3)He magnetic resonance. *Am J Respir Crit Care Med* 2013;187:1104–1109.
32. Narayanan M, Owers-Bradley J, Beardsmore CS, Mada M, Ball I, Garipov R, Panesar KS, Kuehni CE, Spycher BD, Williams SE, *et al*. Alveolarization continues during childhood and adolescence: new evidence from helium-3 magnetic resonance. *Am J Respir Crit Care Med* 2012;185:186–191.
33. Wong PM, Lees AN, Louw J, Lee FY, French N, Gain K, Murray CP, Wilson A, Chambers DC. Emphysema in young adult survivors of moderate-to-severe bronchopulmonary dysplasia. *Eur Respir J* 2008;32:321–328.